CIRP Annals - Manufacturing Technology 72 (2023) 373–376

Contents lists available at ScienceDirect

CIRP Annals - Manufacturing Technology

journal homepage: https://www.editorialmanager.com/CIRP/default.aspx

A framework for hybrid manufacturing cost minimization and preform design

Tony Schmitz (2)[a,b], Gregory Corson[a], David Olvera[b], Christopher Tyler (3)[b], Scott Smith (1)[b,*]

[a] Department of Mechanical, Aerospace, and Biomedical Engineering, University of Tennessee, Knoxville, TN 37996, USA
[b] Manufacturing Science Division, Oak Ridge National Laboratory, Oak Ridge, TN 37830, USA

ARTICLE INFO

Article history:
Available online 3 May 2023

Keywords:
Hybrid manufacturing
Optimization
Preform

ABSTRACT

This paper describes preform design optimization in hybrid additive-subtractive manufacturing. In hybrid manufacturing, the question of what form and what geometry the additive preform should take has largely been a matter of intuition and experience, or trial and error. The choice of a more optimal preform depends on the target parameters, such as stiffness, cost, or lead time. We demonstrate a framework for preform optimization using static stiffness, and then the combined cost of additive and subtractive manufacturing, while respecting stable cutting conditions for the tool-part combination. The procedure is illustrated by comparing three preform geometries for a thin wall.

1. Introduction

In hybrid manufacturing, additive manufacturing (AM) processes are used for layer-by-layer material deposition, and machining is used to remove material from the printed preform to obtain the required surface finishes and dimensional tolerances. Additive preforms are often built close to the desired geometry using a small machining allowance in an attempt to minimize material use (often called the buy-to-fly ratio). However, the resulting preforms may be so flexible that the subsequent (required) machining becomes difficult or impossible. Static and dynamic part deflection may cause surface location error, and chatter may spoil the surface finish of the part. Several researchers have recognized this issue and proposed solutions such as adding sacrificial structures [1,2] or changing the preform thickness [3] to improve preform static stiffness. The previous work in preform design was largely intuitive, and neglected other optimization objectives including dynamic stiffness, manufacturing time, and total cost.

This paper describes: (1) a hybrid manufacturing cost model, considering powder bed AM and machining costs; (2) an efficient method for generating a preform design to withstand cutting forces; and (3) cost-based design selection that provides stable behavior during preform machining. The stability-constrained process planning directly informs the hybrid manufacturing cost model. This, and the approach to generate an initial preform are novel contributions to the state of the art.

2. Hybrid manufacturing cost minimization framework

The hybrid manufacturing cost C_{HM} is presented as the sum of the AM cost C_{AM} and machining cost C_M in Eq. (1).

$$C_{HM} = C_{AM} + C_M \tag{1}$$

With any method of preform manufacturing, there will be ranges and limitations in layer height and bead width that will have to be considered when designing the preform. In this study, laser powder bed fusion was chosen as the AM method due to its high-resolution build capabilities. Alternatively, wire arc AM would provide coarser resolution and reduced preform fidelity, but higher metal deposition rates.

The AM cost model considered in this study is shown in Eq. (2) [4]. Here v_m is the AM deposition volume r_m is the material cost per unit volume $r_{t,\ AM}$ is the machine and operator cost per unit time $\overline{p}_{\ AM}$ is the average electrical power consumption r_e is the electrical power cost per unit time t_{AM} is the deposition time, and $C_{fix,AM}$ is the fixed cost, which does not depend on the operating parameters. Standard industry values were applied in this study and the electrical power was measured.

$$C_{AM} = v_m r_m + (r_{t,\ AM} + \overline{p}_{\ AM} r_e) t_{AM} + C_{fix,AM} \tag{2}$$

The machining cost was modeled using Eqs. (3) to (6) [5]. In Eq. (3) $r_{t,M}$ is the cost per unit time for the machine and operator $\overline{p}_M$ is the average electrical power consumption t_M is the machining time $C_{fix,M}$ is the fixed cost, and C_{tl} is the tooling cost. In Eq. (4) $\overline{F}_t$ is the average tangential force r is the tool radius, and $\overline{p}_a(\Omega)$ is the average electrical power consumption for air cutting as a function of spindle speed. The average tangential cutting force was calculated using Eq. (5) and the average start angle ϕ_s was defined using the average radial depth of cut for down (climb) milling. The machining time was calculated as a

This manuscript has been authored in part by UT-Battelle, LLC under Contract No. DE-AC05-00OR22725 with the DOE. The US Government retains and the publisher, by accepting the article for publication, acknowledges that the US Government retains a non-exclusive, paid-up, irrevocable, world-wide license to publish or reproduce the published form of this manuscript, or allow others to do so, for United States Government purposes. The DOE will provide public access to these results of federally sponsored research in accordance with the DOE Public Access Plan (http://energy.gov/downloads/doe-public-access-plan).

* Corresponding author.
E-mail address: smithss@ornl.gov (S. Smith).

https://doi.org/10.1016/j.cirp.2023.04.051
0007-8506/

function of: 1) path length for an integer number of axial passes; and 2) the feed rate $f = \Omega N_t f_t$ where Ω is the spindle speed N_t is the number of cutting edges, and f_t is the feed per tooth.

$$C_M = (r_{t,M} + \overline{p}_M r_e) t_M + C_{fix,M} + C_{tl} \tag{3}$$

$$\overline{p}_M = \overline{F}_t \Omega r \left(\frac{2\pi}{60}\right) + \overline{p}_a(\Omega) \tag{4}$$

$$\overline{F}_t = \frac{1}{\phi_e - \phi_s} \int_{\phi_s}^{\phi_e} (k_{tc} b f_t s(\phi) + k_{te} b) d\phi \tag{5}$$

The tooling cost C_{tl} is described by Eq. (6), where C_{pt} is the cost per tool, and T is the tool life. A Taylor tool life model can be used to predict tool life, for example.

$$C_{tl} = C_{pt} \left(\frac{t_M}{T}\right) \tag{6}$$

With the hybrid manufacturing cost model in place, the next step is to define the preform geometry. Section 3 discusses one form of generative design for a variety of aerostructure components.

3. Preform generation for uniform static stiffness

The geometry of aerostructure components depends on operational safety and weight minimization. A typical aerospace component, such as the one shown in Fig. 1a, can contain many thin-walled features. Machining of these thin-walled features has been the subject of several prior studies [6–17], aimed at mitigating the primary processing challenges: surface location error and chatter. Thin wall features commonly encountered in aerostructure components include one, two, or three fixed boundaries as displayed in Fig. 1b-1d.

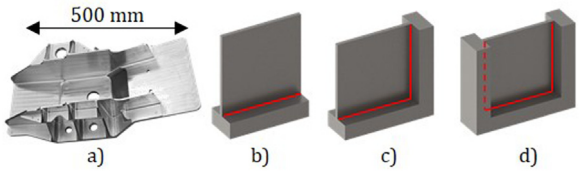

Fig. 1. (a) Example aerostructure component demonstrating, (b) one fixed boundary, (c) two fixed boundaries, and (d) three fixed boundaries.

As an alternative to machining parameter or strategy-based preform design, the proposed method provides a nearly constant stiffness at the top edge of the thin-walled feature. Considering the single fixed boundary in Fig. 1b, the proposed method for generating the preform geometry based on static stiffness includes six steps.

1. The maximum permissible deflection at the top of the thin wall feature is established based on the static deflection tolerance.
2. The tool is selected based on wall or pocket depth, radius between walls, work material, and fillet radius.
3. The cutting force defining parameters for the semi-finishing and finishing operations for the tool-workpiece material combination are selected based only on known performance of the tool assembly.
4. Using a mechanistic force model, the magnitudes of the cutting force components are predicted based on workpiece material cutting coefficients and cutting parameters.
5. Euler-Bernoulli beam theory is used to select the preform thickness as function of thin wall height.
6. Stiffness compensation rules based on stiffness reduction towards width end(s) of the preform are applied.

The cutting force model used for this work has been previously described in detail [18,19]. The cutting force coefficients for Ti-6Al-4 V previously reported in [18] are applied here:

The preform wall is considered as a stepped cantilever beam, using n steps with thickness equal to an integer multiple of the deposition layer thickness, as shown in Fig. 2. Using Castigliano's 2nd theorem [20], the thickness of the first layer can be calculated based on

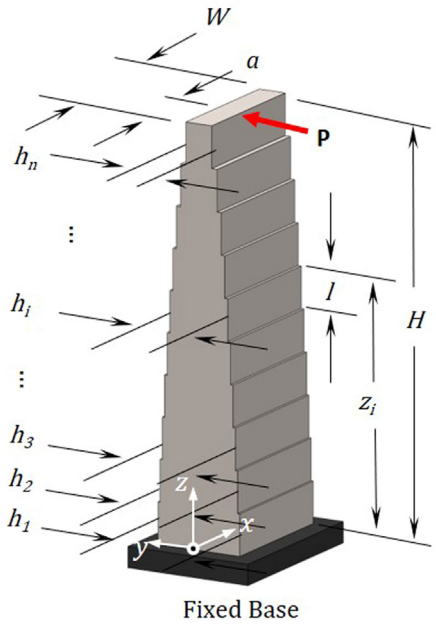

Fig. 2. Stepped beam preform.

maximum permissible deflection and the maximum static cutting force P as:

$$h_n^3 = \frac{4Pl^3}{EW\delta_{max}} \sum_{i=1}^{n} \frac{\left[(1+n-i)^3 - (n-1)^3\right]}{\left(\sqrt{n+1-i}\right)^3} \tag{7}$$

The thickness for all subsequent steps towards the base is then calculated using Eq. (8) which considers bending stress homogeneity along the height of the preform.

$$h_i = \left(\sqrt{n+1-i}\right) \cdot h_n \tag{8}$$

As the beam width W increases, the top corners become more flexible than the top middle and the preform looks less like a cantilever beam. Finite element analysis (FEA) was used to estimate the stiffness variation along the top edge, and the thickness was increased from the middle toward the edges in proportion to the decrease in modeled stiffness. This preform geometry, as shown in Fig. 3(a), provides nearly constant static stiffness along the top edge of the preform. This strategy can be extended to other edge support conditions, and the preform for two fixed boundaries is shown in Fig. 3(b). Here, the preform wall is thicker near the free top corner, but less thick near the fixed top corner.

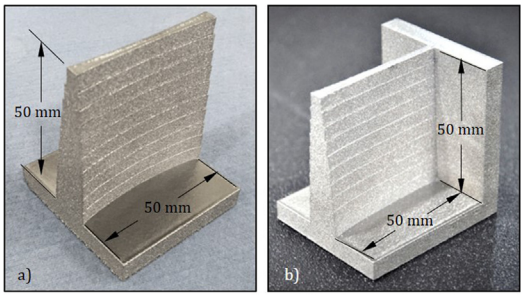

Fig. 3. Ti-6Al-4 V preforms for (a) one fixed boundary, and (b) two fixed boundaries.

4. Milling parameter selection

The minimum static stiffness of the preform is important, but not sufficient for a robust design. Dynamic stiffness is also important to avoid chatter. In this case, impact tests showed that the tool's dynamic stiffness was significantly higher than the dynamic stiffness of the preform, and therefore, the tool was not considered further. As an alternative to measurement, the tool tip dynamic characteristics could also be estimated using receptance coupling substructure analysis (RCSA) [21].

For the preform, the frequency response functions (FRFs) vary with spatial location and change as material is removed during machining. Therefore, these FRFs must be calculated point by point during machining to ensure stability for discrete "in-process" cut stock states.

The in-process preform FRFs in the y direction were simulated using Abaqus™, a commercial FEA software. The wall and overbuilt geometry were modeled separately and meshed with linear hexahedral elements (C3D8R) as shown in Fig. 4. This enabled the overbuilt material to be incrementally removed in the z direction to mimic machining. For each simulation, the first five mode shapes were calculated, and the mass-normalized mode shapes were saved. The preform direct FRF $\frac{Y}{F}(\omega)$ at each grid location was then calculated. Because the modal damping ratios are difficult to predict, measured damping ratios were used.

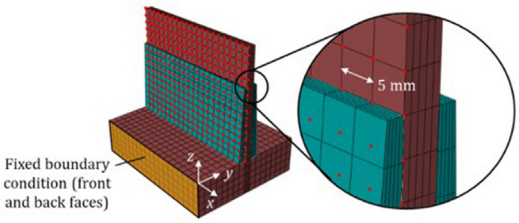

Fig. 4. FEA model for preform FRF simulation, where the grid spacing is 5 mm and the overbuilt material is blue.

Stability maps were calculated at each FEA grid location for each row as the overbuilt geometry was removed from top to bottom. Stability maps were calculated using the predicted FRFs at the top of the overbuilt material, cutting force coefficients, and radial depth of cut (where the preform was machined to its finish dimension in a single pass). The stability maps from all grid locations were then superimposed to identify the minimum value at each spindle speed and to construct a "global" stability map, which ensured stable conditions for the entire machining operation. Based on the global stability map, the final machining conditions were selected. The spindle speed for a safely stable maximum material removal rate (MRR) was chosen.

5. Experimental demonstration

As a demonstration of the preform design and cost minimization framework, three rib preforms were designed and analyzed. The final geometry of the thin rib was 50 mm × 50 mm × 1.25 mm, and the excess volume was added around this geometry. The Ti-6Al-4 V preforms were created using laser powder bed fusion with no support features/material. The preform designs chosen in the comparative study are shown in Fig. 5. The first design was a uniform thickness, where an 8:1 height-to-thickness aspect ratio was selected. The excess thickness was therefore 2.5 mm on each side. The second design was a ramp shape with a top excess thickness of 1 mm and bottom excess of 5 mm. The third design was stepped. At the edge, the thickness varied from 4.3 mm at the top to 13.5 mm at the bottom. At the center, the thickness varied from 2.5 mm at the top to 7.9 mm at the bottom. The excess volumes (not including the rib and base) resulted in preform volumes of 12,500 mm^3, 15,000 mm^3, and 11,475 mm^3.

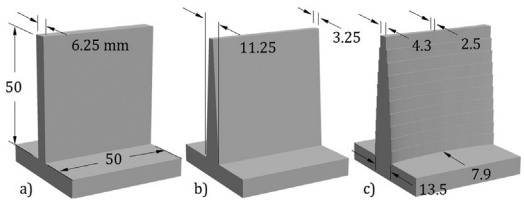

Fig. 5. Three preform designs: (a) constant thickness, (b) ramp, and (c) stepped uniform static stiffness.

The constant thickness design (Fig. 5a) has low material cost based on volume, but due to the structural dynamics, the lower volume may cost more to machine. The stiffness of the stepped uniform preform (Fig. 5c) is shown in Fig. 6, which compares the predicted

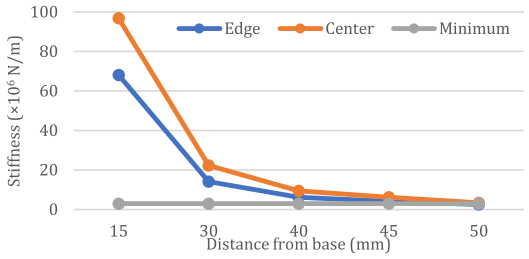

Fig. 6. Ti-6Al-4 V stepped preform static stiffness at the wall center and wall edge as a function of the distance from the base (height).

static stiffness to the minimum target value of 3×10^6 N/m. It is seen that the minimum stiffness, located at the top edge, exceeds the minimum stiffness target, as desired. Static stiffness estimates from FRF testing agreed to within 15%.

Because the workpiece is titanium, a conservative cutting speed of 90 m/min was selected. At low cutting speeds, process damping plays an important role in maximizing available (stable) axial depths of cut [22,23]. For this reason, this study considered process damping when estimating the global stability boundary.

To provide consistency in choosing the operating parameters from the global stability maps with process damping, a limiting axial depth of 5 mm was chosen, then the highest stable spindle speed at that depth was selected. The 5 mm depth was chosen to respect the static deflection threshold. Fig. 7 displays the global stability boundary comparison and machining parameters for all three designs during the finishing operation. The stability boundaries were calculated using MLI's TXF software [24] with a process damping wavelength of 0.4 mm [25].

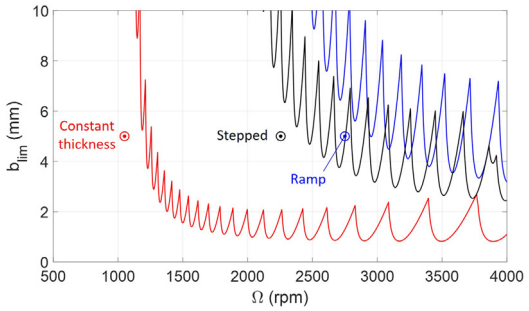

Fig. 7. Global stability maps showing allowable axial depth, blim, versus spindle speed, Ω. The operating parameters for the three preform designs are identified by the circles.

Fig. 7 highlights the influence of the preform's fundamental natural frequency on the process damping behavior. The constant thickness preform has more mass and the lowest natural frequency, which causes the process damping effect to apply at a lower spindle speed range. The preform with the least mass (ramp) has the highest fundamental natural frequency, which makes the process damping effect active at a higher spindle speed range. The stepped preform has a process damping range between these two. It is interesting to note that if the preform material was aluminum, a much higher surface speed would be permissible and, consequently, a lower natural frequency would be preferred to make the stable zones between lobes accessible within the machine's spindle speed range. Process damping would have little influence at the higher cutting speed.

Validation tests show that the static stiffness preform design and cost minimization produced a wall with (excess) thickness deviation from the nominal between 36 µm and 65 µm; the machined thin rib is shown in Fig. 8. The surface roughness was measured at 15 different locations for each side. The results were 1.5 µm ≤ Rz ≤ 3 µm and 0.18 µm ≤ Ra ≤ 0.57 µm.

The final costs associated with the three designs are shown in Fig. 9. It is seen that the stepped uniform static stiffness design results in the lowest additive, machining, and hybrid manufacturing costs. The ramp design was the stiffest and had a higher natural frequency than the others, but the additional material and similar machining parameters resulted in a higher overall hybrid manufacturing cost than the stepped uniform static stiffness design. The stepped uniform

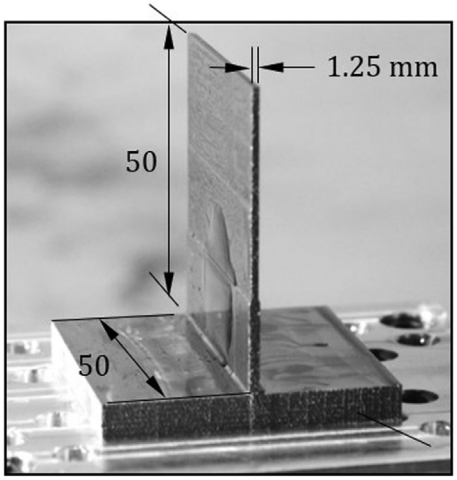

Fig. 8. Thin rib machined from stepped uniform static stiffness preform.

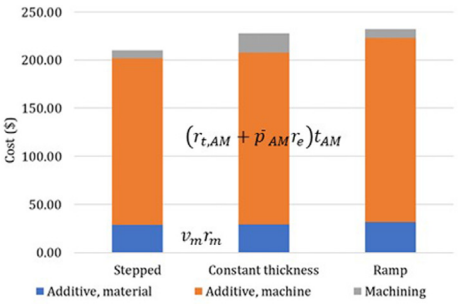

Fig. 9. Hybrid manufacturing costs for the three preform designs. The Eq. (2) contributions are individually identified.

Table 1
Ti-6Al-4 V mechanistic cutting force coefficients [18].

	TANGENTIAL	RADIAL	AXIAL
SHEARING	K_{tc} 1815N/mm^2	K_{rc} 646N/mm^2	K_{ac} 702N/mm^2
PLOUGHING	K_{te} 29.7N/mm	K_{re} 55.7N/mm	K_{ae} 1.8N/mm

static stiffness preform reduced the hybrid manufacturing cost by 8.4% and 10.5% compared to the constant thickness and ramp preforms (Table 1).

6. Conclusions

This paper compared three hybrid additive-subtractive preforms for a thin-walled part with one fixed constraint. The preforms were created in Ti-6Al-4 V using laser powder bed fusion. Two intuitive and industrially common preforms: a constant thickness prismatic preform and a triangular prism preform (ramp), were compared to a preform that used a stiffness-based design strategy. For the latter, a new preform geometry (stepped) was designed with nearly constant static stiffness along the top edge by modifying the thickness along the wall width. In each case, the cutting conditions were chosen so that stable machining conditions were maintained at every spatial location on the thin-walled parts from top to bottom as metal was removed.

For these preforms, the part was considerably more flexible than the tool, so the preform dynamics dominated the stability maps. The critical stability limit at the most flexible preform location was between 1 mm and 3 mm. Because the preform was titanium, low cutting speeds were required to avoid high tool wear rates and the spindle speed was selected in the process damping zone.

For the selected part geometry, the ramp and stepped preform designs had higher fundamental natural frequencies than the constant thickness design, which enhanced the process damping effect and provided higher metal removal rates. The static stiffness of the stepped preform was higher, which provided better surface location accuracy than the other two preform designs.

In the cost analysis, the additive manufacturing cost was dominant for all three preforms. The hybrid manufacturing cost for the stepped preform was 10.5% lower than the ramp preform and 8.4% lower than the constant thickness preform. The stiffness-based preform design and cost-based preform selection provided a framework for optimizing hybrid manufacturing with respect to total cost. For other applications, including aerospace aluminum alloys, the cost-based framework can be applied to select the best process combinations, part designs, and machining parameters.

Declaration of Competing Interest

The authors declare that they have no known competing financial interests or personal relationships that could have appeared to influence the work reported in this paper.

Acknowledgment

The authors gratefully acknowledge the support of the DOD, Industrial Base Analysis and Sustainment program.

References

[1] Smith S, et al. (2012) Sacrificial Structure Preforms for Thin Part Machining. *Annals of the CIRP* 61(1):379–382.
[2] Vaughan D, Saldana C, Kurfess T, Nycz A (2022) Implementation of Sacrificial Support Structures for Hybrid Manufacturing of Thin Walls. *Journal of Manufacturing and Materials Processing* 6(4):70.
[3] Tunc LT, Zatarain M (2019) Stability Optimal Selection of Stock Shape and Tool Axis in Finishing of Thin-Wall Parts. *Annals of the CIRP* 68(1):401–404.
[4] Rickenbacher L, Spierings A, Wegener K (2013) An Integrated Cost-Model for Selective Laser Melting (SLM). *Rapid Prototyping Journal* 19(3):208–214.
[5] Tlusty J (1999) *Manufacturing Processes and Equipment*, Prentice Hall. ISBN 978-0201498653.
[6] Budak E, Altintas Y (1995) Modeling and Avoidance of Static Form Errors in Peripheral Milling of Plates. *International Journal of Machine Tools and Manufacture* 35:459–476.
[7] Tlusty J, Smith S, Winfough W (1996) Techniques for the use of Long Slender End Mills in High-Speed Milling. *Annals of the CIRP* 45(1):393–396.
[8] Smith S, Dvorak D (1998) Tool Path Strategies for High Speed Milling Aluminum Workpieces with Thin Webs. *Mechatronics* 8:291–300.
[9] Ning H, Zhigang W, Chengyu J, Bing Z (2003) Finite Element Method Analysis and Control Stratagem for Machining Deformation of Thin-Walled Components. *Journal of Materials Processing Technology* 139:332–336.
[10] Ratchev S, et al. (2023) Milling Error Prediction and Compensation in Machining of Low-Rigidity Parts. *International Journal of Machine Tools and Manufacture* 44:1629–1641.
[11] Bravo U, Altuzarra O, López de Lacalle LN, Sánchez JA, Campa FJ (2005) Stability Limits of Milling Considering the Flexibility of the Workpiece and the Machine. *International Journal of Machine Tools and Manufacture* 45:1669–1680.
[12] Thevenot V, Arnaud L, Dessein G, Cazenave-Larroche G (2006) Influence of Material Removal on the Dynamic Behavior of Thin-Walled Structures in Peripheral Milling. *Machining Science and Technology* 10(3):275–287.
[13] Rai JK, Xirouchakis P (2008) Finite Element Method Based Machining Simulation Environment for Analyzing Part Errors Induced During Milling of Thin-Walled Components. *International Journal of Machine Tools and Manufacture* 48(6):629–643.
[14] Chen W, Xue J, Tang D, Chen H, Qu S (2009) Deformation Prediction and Error Compensation in Multilayer Milling Processes for Thin-Walled Parts. *International Journal of Machine Tools and Manufacture* 49(11):859–864.
[15] Gang L (2009) Study on Deformation of Titanium Thin-Walled Part in Milling Process. *Journal of Materials Processing Technology* 209(6):2788–2793.
[16] Arnaud L, Gonzalo O, Seguy S, Jauregi H, Peigné G (2011) Simulation of Low Rigidity Part Machining Applied to Thin-Walled Structures. *The International Journal of Advanced Manufacturing Technology* 54(5):479–488.
[17] Schmitz T, Honeycutt A (2017) Analytical Solutions for Fixed-Free Beam Dynamics in Thin Rib Machining. *Journal of Manufacturing Processes* 30:41–50.
[18] Altintas Y (2000) Manufacturing Automation: Metal Cutting Mechanics. *Machine Tool Vibrations, and CNC Design*, Cambridge University Press. ISBN 10:0521659736.
[19] Schmitz T, Smith S (2009) *Machining Dynamics, Frequency Response to Improved Productivity*, Springer. ISBN 978-0-387-09644-5.
[20] Hibbeler RC (2003) *Mechanics of Materials*, 5th ed. Pearson Education Inc.. ISBN 0-13-008181-7.
[21] Schmitz T, Donaldson R (2000) Predicting High-Speed Machining Dynamics by Substructure Analysis. *Annals of the CIRP* 49(1):303–308.
[22] Tyler C, Schmitz T (2014) Process Damping Milling Model Database. In: *Proceedings of the NAMRI/SME*, .
[23] Munoa J, et al. (2016) Chatter Suppression Techniques in Metal Cutting. *Annals of the CIRP* 65(2):785–808.
[24] Manufacturing Laboratories Inc., https://mfg-labs.weebly.com/, Accessed 12 January 2023.
[25] Turner S (2011) Process Damping Parameters. *IOP Conference Series: Materials Science and Engineering* 26(1):012008.